Water-dispersible Gadolinium Oxide Nanoplates as an Effective Positive Magnetic Resonance Imaging Contrast Agent

Nguyen Thi Thuy Khue,*[a, b] Le Thi Thanh Tam,*[c] Ngo Thanh Dung,[c] Le The Tam,[d] Nguyen Xuan Chung,[e] Nguyen Thi Ngoc Linh,[f] Nguyen Dinh Vinh,[f] Bui Minh Quy,[f] and Le Trong Lu*[a, c]

Gadolinium oxide (Gd_2O_3) nanoplates have been successfully synthesized by thermal decomposition method in the presence of oleic acid and oleylamine as surfactants. As a result, the nanoplates have average edge length and thickness around 10 nm and 1.1 nm, respectively. The hydrophobic OA/OM capped Gd_2O_3 nanoplates were encapsulated with amphiphilic poly (maleic anhydride-alt-1-octadecene) polymer (PMAO) for phase transfer into aqueous media. The obtained Gd_2O_3@PMAO showed a hydrodynamic size of 32 nm with good dispersion in water solvent and stable in wide range of pH (pH = 2 ÷ 11) and at electrolyte concentrations as high as NaCl 380 mM. In addition, the in vitro toxicity tests confirmed the biocompatibility of Gd_2O_3@PMAO nanoplates. The magnetic resonance imaging (MRI) result exhibited the r_1 of Gd_2O_3@PMAO nanoplates (16.95 $mM^{-1}s^{-1}$) is four times higher than that of clinically used Gd-DTPA. These results suggest that the PMAO coated -Gd_2O_3 nanoplates are potential T_1 contrast agents for in vivo MRI application.

Introduction

MRI is one of the most powerful molecular imaging techniques with outstanding advantages, such as, fast scan speed, unlimited tissue penetration, high spatial resolution and no radiochemical damage.[1–3] However, the main drawback of this diagnostic technique is its relatively low sensitivity, therefore it is necessary to use contrast agents (CAs) to improve diagnostic accuracy, especially for diagnosis of tumors.[4] Currently, approximately 40–50% of clinical MRI scans are performed with the assistance of CAs.[5–7] Until now, two types of CAs in use clinically are paramagnetic gadolinium -based chelates for T_1-weighted MRI (positive CAs) and superparamagnetic iron oxide nanoparticles for T_2-weighted MRI (negative CAs).[8,9] These contrast agents operate by interacting with the surrounding water protons to shorten their relaxation times, resulting in enhanced contrast in the regions of interest with the brighter signal in the T_1-weighted images or darker signal in T_2-weighted images.[10] However, T_1 contrast agents are more commonly used in clinical practice because their brighter signal can be easily distinguished from other pathogenic or biological conditions.[11]

Gadolinium (Gd)-based chelates such as gadolinium-diethylenetriamine pentaacetic acid (Gd-DTPA) and gadoterate meglumine (Gd-DOTA) are commonly used as positive MRI contrast agents due to seven unpaired electrons in gadolinium ion, thus they exhibit high magnetic moment and long electronic relaxation time with longitudinal relaxivity (r_1) values of 3–5 $mM^{-1}s^{-1}$ suitable for MRI contrast enhancement.[12–14] Notwithstanding, Gd-based chelates still have some obstacles. They exhibited a short blood circulation duration and rapid excretion due to their low molecular weights.[15,16] In addition, the low local concentration of Gd^{3+} ions per each chelate leads to the need for a large amount of contrast agent to complete the MRI scan. Most important, the release of free Gd (III) ions from Gd-chelates was reported to be responsible for nephrogenic systemic fibrosis (NSF) in patients.[17–20] In contrast, Gd_2O_3 nanostructures are considered as potential candidates to replace Gd-chelate compounds for T_1-weighted MRI because of their high longitudinal water proton spin relaxivity (r_1).[21–23] The Gd_2O_3 nanocrystals contain a high payload of Gd^{3+} ions on their surface for water hydration, so the longitudinal relaxation is significantly larger than that of Gd-chelates, which has great

[a] Dr. N. Thi Thuy Khue, Dr. L. Trong Lu
     Graduate University of Science and Technology,
     Vietnam Academy of Science and Technology,
     18 Hoang Quoc Viet, Hanoi, Vietnam
     E-mail: nguyenthithuykhue@gmail.com
[b] Dr. N. Thi Thuy Khue
     Haiphong University of Medicine and Pharmacy,
     72A Nguyen Binh Khiem, Ngo Quyen,
     Hai Phong, Vietnam
[c] MSc. L. T. Thanh Tam, Dr. N. Thanh Dung, Dr. L. Trong Lu
     Institute for Tropical Technology,
     Vietnam Academy of Science and Technology,
     18 Hoang Quoc Viet, Hanoi, Vietnam
     E-mail: ltlu@itt.vast.vn
            thanhtam.le95pt@gmail.com
[d] Dr. L. The Tam
     Vinh University, 182 Le Duan,
     Vinh City, Vietnam
[e] Dr. N. Xuan Chung
     Department of Physics,
     Hanoi University of Mining and Geology,
     18 Pho Vien, Bac Tu Liem, Hanoi, Vietnam
[f] Dr. N. Thi Ngoc Linh, Dr. N. Dinh Vinh, Dr. B. Minh Quy
     Thai Nguyen University of Sciences,
     Tan Thinh Ward, Thai Nguyen City
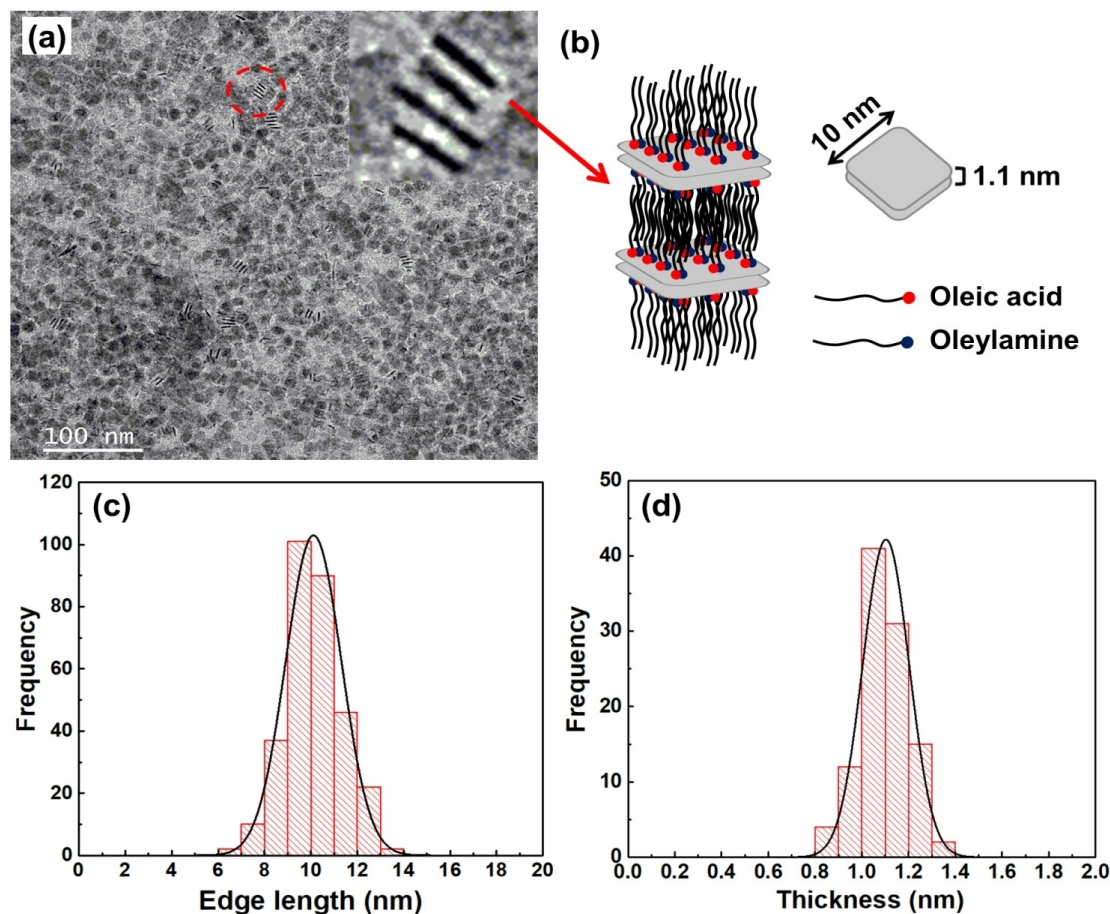   25000, Thai Nguyen, Vietnam

Figure 1. (a) TEM image of Gd_2O_3 nanoplates, (b) illustration of OA/OM capped-Gd_2O_3 nanoplates and (c) Edge length distribution histogram and (d) Thickness distribution histogram of Gd_2O_3 nanoplates.

significance in reducing the dose of Gd^{3+} ions injected into the body.[20,24,25] Furthermore, Gd_2O_3 nanostructures can minimize the leaching of Gd^{3+} ions on account of their stable solid crystal structure thereby limiting possible toxicity.[26,27]

Because of above advantages, much research on gadolinium oxide as effective contrast agents in preclinical and clinical applications has been reported in recent years.[25,27–32] In particular, ultrasmall gadolinium oxide nanostructures have been demonstrated to significantly enhance the longitudinal relaxation presumably due to a high density of Gd^{3+} ions on each particle's surface as the particle size decreases.[4,26,33–35] This reveals that a high performance T_1 contrast agent can be made by designing Gd_2O_3 nanostructures with a high surface-to-volume (S/V) ratio to offer more surface paramagnetic Gd^{3+} ions for water hydration, resulting in enhanced contrast effect. Among the various nanostructures of Gd_2O_3, ultrasmall Gd_2O_3 nanoparticles and nanoplates with large specific surface area have attracted considerable attention.[19,36] Especially, the 2D Gd_2O_3 nanoplates are much preferred for T_1-weighted MRI as they are formed by assembly of single layer of unit cells, and thus have higher surface area than that of conventional spherical nanostructures with the same volume.[36–39] Furthermore, 2D nanostructures can provide a pathway for the close
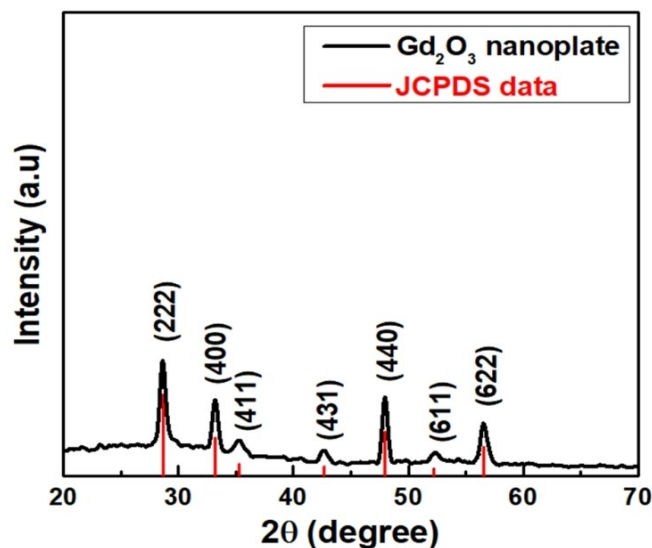

Figure 2. XRD pattern of Gd_2O_3 nanoplates.

approach of water molecules through their unblocked edges because the surface ligands tend to bind to the larger faces of
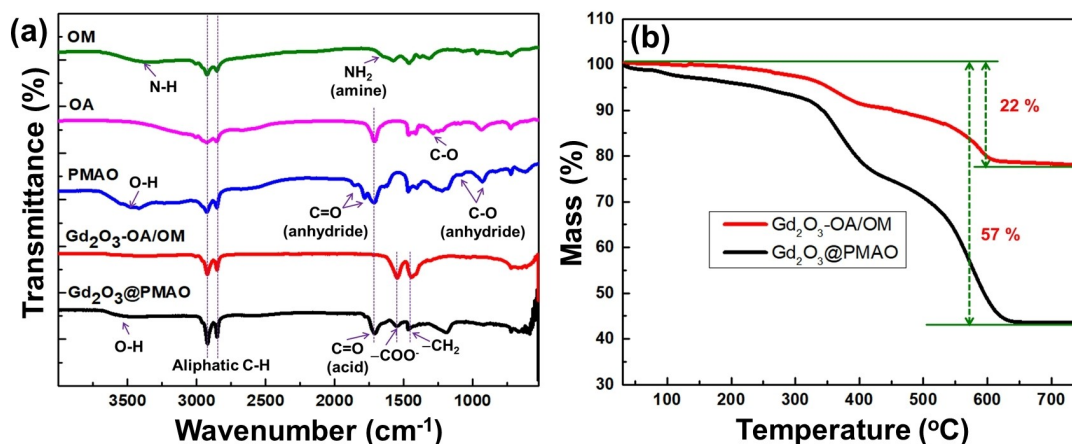
Figure 3. (a) FT-IR spectra of Gd_2O_3 nanoplates capped with OA/OM and PMAO molecules, (b) TGA scans of Gd_2O_3 nanoplates before and after encapsulation with PMAO.
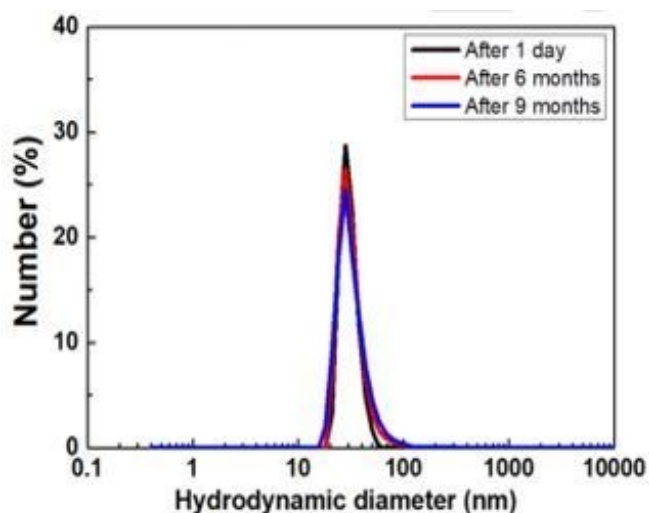

Figure 4. DLS pattern of Gd_2O_3@PMAO nanoplates after 1 day, 6 months and 9 months of storage.
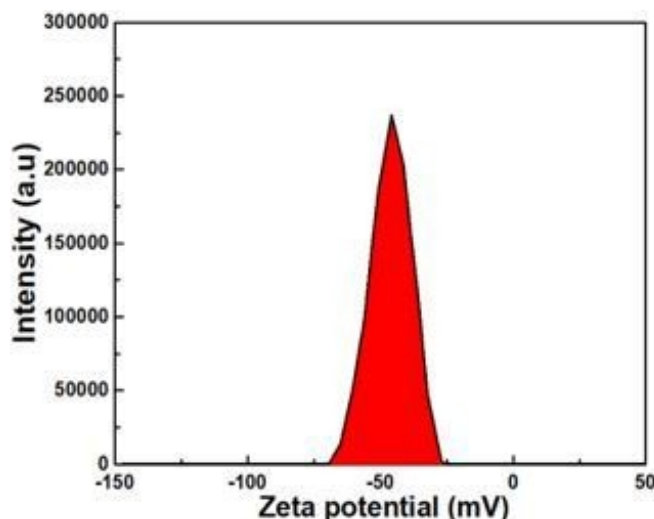

Figure 5. Zeta potential of Gd_2O_3@PMAO nanoplates.

nanoplates, resulting in the T_1 relaxation was significantly enhanced.[40–42]

In order to be used as T_1 MRI contrast agents, Gd_2O_3 nanoplates should be non-toxic, well dispersed and stable in aqueous media. Thus far, most of the synthesis methods of Gd_2O_3 nanoplates are often conducted in organic-phase and use hydrophobic surface ligands to control of their morphology anddimension.[43,44] So, it is necessary to modify the surface of hydrophobic Gd_2O_3 nanoplates with hydrophilic and biocompatible ligands. Here, a more hydrophilic ligands not only supports Gd_2O_3 nanoplates to disperse well in aqueous media, but also provides a higher r_1 value because they can allow more water molecules to access and interact with Gd^{+3} ions on particle surface.[19,26,31] Recently, amphiphilic polymers have emerged as efficient biocompatible coating agents with the ability to improve the stability of the nanoparticles (NPs) and

facilitate subsequent surface functionality. As being an amphiphilic biodegradable polymer, poly (maleic anhydride-alt-1-octadecene) (PMAO) is a cost-effective strategy for transferring hydrophobic NPs into aqueous media.[45,46] PMAO polymers as a bio-responsive shell encapsulate the hydrophobic NPs to control the surface charge and cytocompatibility of NPs in vivo. The phase transfer mechanism is based on ability to interact with both lipophilic and hydrophilic molecules of PMAO due to its structure consisting of both polar and nonpolar parts. Specifically, the PMAO molecules are attached to the surface of NPs through the interaction between the hydrocarbon chains of the polymer and those of the NP capping, whilst the hydrophilic anhydride groups of PMAO are pointed outward to the solution forming a hydrophilic surface to make NPs well-dispersed in water or polar solvents. The anhydride groups can be readily hydrolyzed, resulting in the formation of free carboxylate moieties that provide electrostatic stability to the
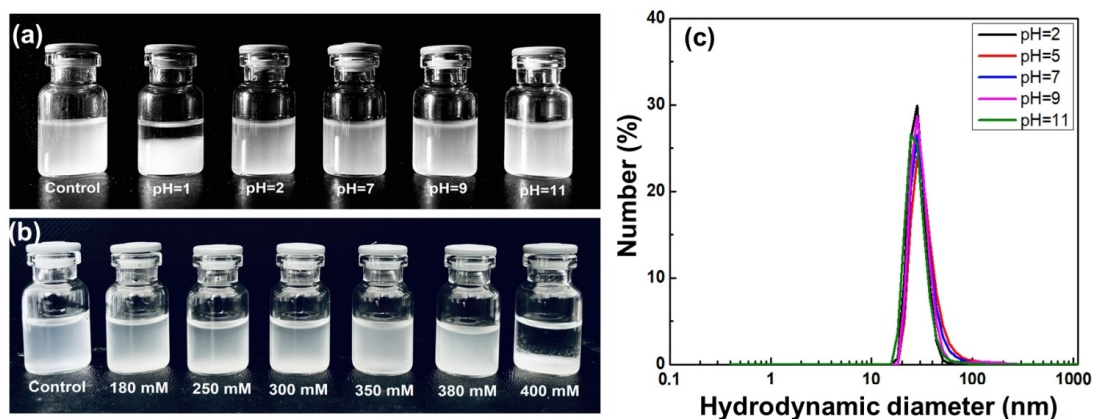
ChemistrySelect

Research Article
doi.org/10.1002/slct.202202062

Chemistry Europe
European Chemical
Societies Publishing

Figure 6. The stability test of PMAO coated Gd_2O_3 nanoplates at different pH conditions (a) and various NaCl concentrations (b) compared with a control sample has $pH = 7$ and $[NaCl] = 0$ M; DLS patterns of Gd_2O_3@PMAO colloidal at different pH conditions (c).
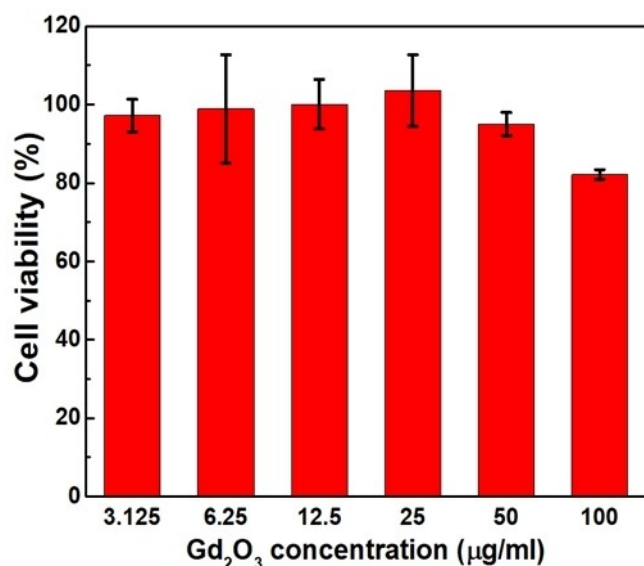

Figure 7. Plot of HEK293 cell viabilities incubated with different concentrations of Gd_2O_3@PMAO nanoplates evaluated by MTT assay after 48 h.

colloid. Besides, the presence of carboxylate groups as an anchor allows conjugation with other biomolecules or ligands for biomedical applications.[47,48]

In this study, we report a facile method to synthesize of ultrathin Gd_2O_3 nanoplates encapsulated with PMAO polymer (Gd_2O_3@PMAO) as an effective-contrast agent with good biocompatibility and improved T_1 contrast effect. The characterizations of the obtained sample such as size, morphology and surface properties were investigated by using transmission electron microscopy (TEM), X-ray diffraction (XRD), Fourier-transform infrared spectroscopy (FT-IR), thermogravimetric analysis (TGA), dynamic light scattering (DLS) and Zeta potential measurements. The MRI result of Gd_2O_3@PMAO nanoplates exhibited the maximum r_1 value of 16.95 $mM^{-1}s^{-1}$, which is four times higher than that of Gd-DTPA commercial contrast agent. The cytotoxicity test on HEK293 cell line proved

that the Gd_2O_3@PMAO nanoplates are relatively safe for bioapplications.

Results and Discussion

Characterizations of Gd_2O_3 nanoplates

In this work, Gd_2O_3 nanoplates were synthesized by thermal decomposition method with high temperature of 320 °C in the presence of oleic acid (OA) and oleylamine (OM) as surfactants. The OA and OM ligands were bound to the Gd_2O_3 nanoplates to prevent self-aggregation of nanoplates via inter-particle dipolar- dipolar repulsive force; in which OA tends to attach on the surface of oxide nanocrystals more strongly than OM due to its higher oxophilicity. Therefore when parameters such as temperature and reaction time were remained constant, the ratio of OA to OM plays an important role in the formation and growth of ultra-thin nanoplates. In this study, the OA/OM ratio of 1:1 was used to achieve dimensional control of Gd_2O_3 nanoplates. The reaction pathway for the synthesis of Gd_2O_3 nanoplates is shown in Scheme 1.

The morphology of as-prepared Gd_2O_3 nanoplates was determined using TEM. As can be seen from the TEM image of Figure 1, the morphology of the obtained Gd_2O_3 particles is square nanoplate with an average face dimension of 10 nm and thin edges approximately 1.1 nm. Besides, the edge length and thickness distribution of the Gd_2O_3 nanoplates are relatively uniform, as demonstrated in Figure 1c,d.

The crystalline phase structure of the as-prepared Gd_2O_3 nanoplates was identified by XRD analysis. Figure 2 shows the XRD pattern of the obtained Gd_2O_3 nanocrystals with hydrophobic surfactant and the vertical bars below are the corresponding standard card of Gd_2O_3. It can be seen the Gd_2O_3 sample exhibits peaks located at the 2θ angle of 28.6°; 33.2°; 35.3°; 42.7°; 47.9°; 52.2°; 56.5° corresponding to the (222), (400), (411), (431), (440), (611) and (622) planes of the cubic crystal structure with unit cell parameters $a = b = c = 10.8012$ Å. This obtained result is similar to some previous reports about Gd_2O_3
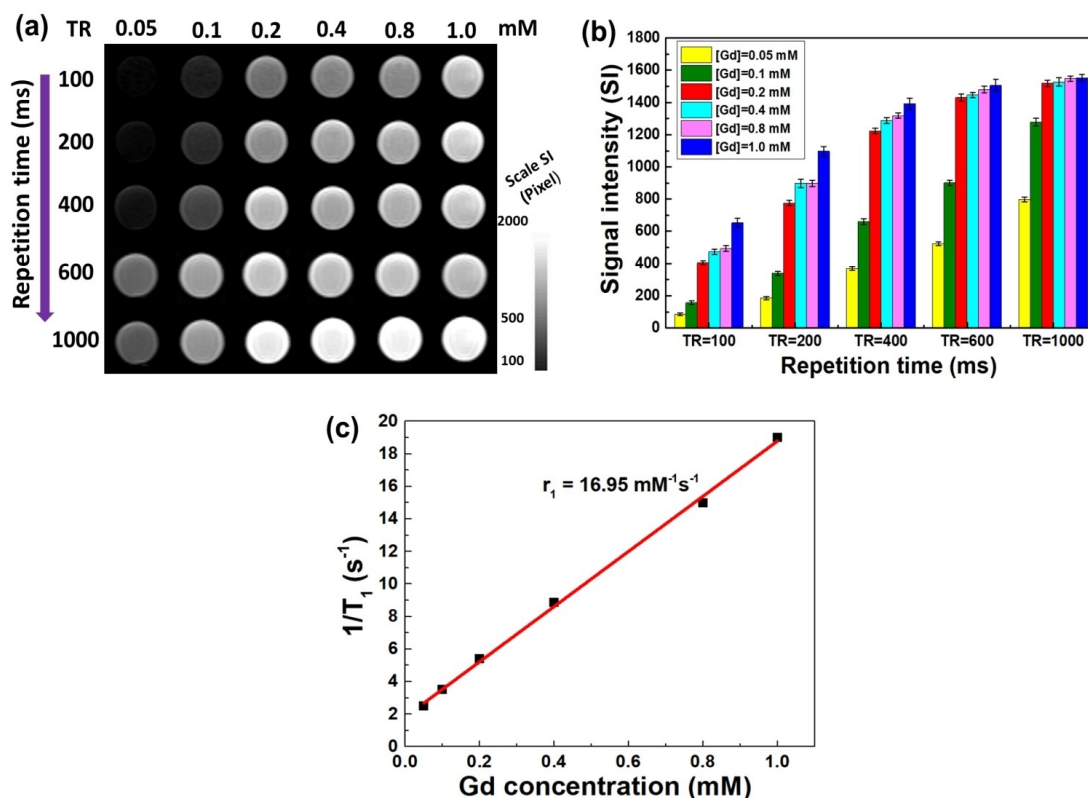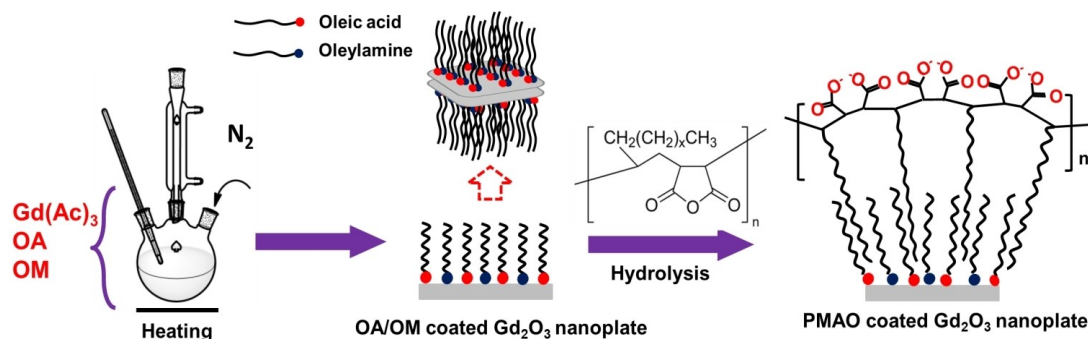
Figure 8. (a) T_1-weighted images of Gd_2O_3@PMAO nanoplates, (b) Plot of T_1 signal intensity corresponding to different TR and Gd concentrations, (c) Longitudinal relaxation of Gd_2O_3@PMAO as a function of Gd concentration.

Scheme 1. Schematic illustration of the fabrication of 2D Gd_2O_3@PMAO nanoplates for T_1-weighted MRI.

nanoplates. For example, Zhow et al. successfully synthesized Gd_2O_3 nanoplates with a typical cubic phase (a = 10.8 Å) rather than monoclinic structure.[36] By a similar method, Stinnett et al. prepared Gd_2O_3 nanoplates with the presence of cubic and monoclinic phase, however the contributions of monoclinic Gd_2O_3 phase to the XRD pattern is minor.[40] In this study, our obtained XRD spectrum only displays the diffraction peaks characteristic for the cubic phase of Gd_2O_3 without any other phase, indicating that the obtained Gd_2O_3 nanoplates have high phase purity, or it also can be because the content of the monoclinic Gd_2O_3 phase is too small to be detected by the XRD

device. Generally, comparing with the standard data, the X-ray peak positions and intensities generally match well with the reference (PDF Card No.: 2106881).

In this work, the hydrophobic OA/OM capped Gd_2O_3 nanoplates were transferred into water by encapsulating with amphiphilic PMAO polymer. The interaction between OA, OM and PMAO molecules for the stabilization of Gd_2O_3 nanoplates was investigated by FT-IR and TGA analyses.

Figure 3a shows FT-IR spectra for the Gd_2O_3 nanoplates capped with OA/OM and PMAO and the reference spectrum for pure OA, OM and PMAO. It can be seen that all samples

ChemistrySelect

Research Article
doi.org/10.1002/slct.202202062

Chemistry Europe
European Chemical
Societies Publishing

exhibited absorption peaks at 2850 and 2920 cm^{-1}, which can be assigned to stretching vibration of aliphatic C–H bonds. In FT-IR spectrum of OA/OM-capped Gd$_2$O$_3$ nanoplates, no absorption peaks were found characteristic for the carbonyl group of oleic acid as well as the amine group of oleylamine, indicating the absence of free –COOH and –NH$_2$ groups on the surface of Gd$_2$O$_3$ nanoplates. Instead, the appearance of peaks at 1548 cm^{-1} and 1442 cm^{-1} represents the asymmetric COO$^-$ stretching and CH$_2$ bending mode, suggesting that the acid-base complex which was formed by the reaction between oleic acid and oleylamine bonded to the Gd$_2$O$_3$ nanoplates. For sole PMAO, the absorption peaks at 1785 cm^{-1} and 1860 cm^{-1} were attributed to the symmetric and asymmetric stretching vibration of the C=O bond in the anhydride groups. In addition, the presence of the anhydride C–O vibrations at 1083 cm^{-1} and 925 cm^{-1} was also observed. For PMAO encapsulated Gd$_2$O$_3$ nanoplate sample, FT-IR data exhibits enhanced intensity of absorption bands at 2850 and 2920 cm^{-1}, demonstrating the conjugation of PMAO. In addition, the disappearance of the anhydride C=O vibrations at 1785 cm^{-1} and 1860 cm^{-1} and the formation of peak at 1712 cm^{-1} corresponding to the carboxylic acid C=O stretching vibrations, indicating the hydrolysis of the anhydride rings of PMAO can be observed.

The presence of PMAO molecule on the surface of Gd$_2$O$_3$ nanoplates was also further confirmed by TGA analysis. In addition, the information about the proportion of Gd$_2$O$_3$ nanoplate cores and surfactant layer in the sample is also provided through the TGA heating curves. Figure 3b shows the TGA thermal analysis curve of Gd$_2$O$_3$ nanoplates before and after PMAO encapsulation. Here, the obtained TGA data indicates that the total weight loss of OA/OM and PMAO capped- Gd$_2$O$_3$ nanoplates is 22% and 57%, respectively. For the Gd$_2$O$_3$@OA/OM case, only a one-step mass loss process (22%) in the temperature between 300–600 °C can relate to the decomposition of the OA/OM complex coated around Gd$_2$O$_3$ core. Meanwhile, the thermogram of the Gd$_2$O$_3$@PMAO sample shows a two-steps weight loss process. It can be observed that the first weight loss at temperatures below 200 °C corresponds to the evaporation of adsorbed water or solvents. The second weight loss of about 52% at higher than 300 °C can be assigned to the decomposition of OA/OM complex and PMAO. Thus, the weight percentage of Gd$_2$O$_3$ core, OA/OM and PMAO of the as-synthesized sample obtained from the TGA data is 43, 22 and 30%, respectively. The obtained results in the current study on the surface structure of Gd$_2$O$_3$@PMAO nanoplates are similar to that of our previous publications on Fe$_3$O$_4$ and CoFe$_2$O$_4$ nanoparticle systems.[49,50]

The colloidal stability of PMAO encapsulated Gd$_2$O$_3$ nanoplates was confirmed with DLS. Figure 4 presents the results of hydrodynamic diameter analysis of Gd$_2$O$_3$@PMAO nanoplates in water after 1 day, 6 months and 9 months of the solution preparation. The obtained results show that the average hydrodynamic diameter of the Gd$_2$O$_3$@PMAO nanoplates after 1 day and more than 9 months of storage is almost unchanged with only one peak at around 32 nm and a narrow size distribution on the DLS spectra were observed, demonstrating

the monodisperse and high colloidal stability of the PMAO polymer coated Gd$_2$O$_3$ nanoplates.

Besides, the Zeta potential value of Gd$_2$O$_3$@PMAO sample was found to be −47 mV in aqueous media (Figure 5), indicating the negative charge biomolecules adhere onto the surface of the Gd$_2$O$_3$ nanoplates, which further confirmed that the Gd$_2$O$_3$ nanoplates had been successfully encapsulated into PMAO polymer. Simultaneously, this high value also confirmed good colloidal stability.

In addition, the stability of Gd$_2$O$_3$@PMAO in various media is tested under different pH conditions and NaCl concentrations. The obtained results are shown in Figure 6, in which the control sample has pH = 7 and salt concentration is zero. As shown in Figure 6a–b, it can be observed that there are no aggregations of the sample over a wide pH range from 2 to 11, as well as at the NaCl concentrations up to 380 mM.

Cellular cytotoxicity test

The cytotoxicity experiments were performed *in vitro* with normal HEK293 cell line by using standard MTT assay. As shown in Figure 7, it could be found that the cell viability remained above 80% at Gd$_2$O$_3$ doses of up to 100 μg/mL for 48 h of incubation. The optical microscope images of HEK293 cell indicate that the cells exhibit the good adhesion with morphology of cells was not different from control sample even at the highest concentration of Gd$_2$O$_3$ nanoplates (Figure S1). This cell viability data indicated that the Gd$_2$O$_3$@PMAO nanoplates are not toxic for the tested Gd$_2$O$_3$ concentration range and suitable for *in vivo* applications.

In vitro T$_1$-weighted magnetic resonance imaging

In order to evaluate the potential of the as-prepared Gd$_2$O$_3$@PMAO nanoplates as an T$_1$-weighted MRI contrast agent, the T$_1$ measurements of the sample with a series of Gd concentrations were performed on a 1.5 T MR scanner. The obtained results are shown in Figure 8. It can be observed from Figure 8a–b that T$_1$ relaxation time depends on the Gd concentration. The T$_1$ image of the Gd$_2$O$_3$@PMAO nanoplates became brighter with the increasing of Gd (III) concentration from 0.05 to 1.0 mM. Besides under a constant Gd concentration, the T$_1$ signal intensity increased with the repetition time (TR). Figure 8c shows the longitudinal relaxation rate of the Gd$_2$O$_3$@PMAO nanoplates as a function of Gd concentration. The obtained data reveals the linearly proportional relation between 1/T$_1$ and Gd concentration. The longitudinal relaxation (r$_1$), which is characterized by the slope of the 1/T$_1$ versus Gd$_2$O$_3$ concentration, is calculated to be 16.95 mM^{-1}s^{-1}. The obtained r$_1$ value for our Gd$_2$O$_3$ nanoplates is about four times higher than that of commercial contrast agent Magnevist (Gd-DTPA, r$_1$ = 4.1 ± 0.2 mM^{-1}s^{-1}),[51] and it is also greater than most of previously reported CAs based on Gd.[6,52–56] The high r$_1$ value of Gd$_2$O$_3$ nanoplates is attributed to the significant contribution of their 2D structure with larger surface area, which provides more Gd atoms for interaction to water molecules, shortening the longitudinal relaxation time and

ChemistrySelect

Research Article
doi.org/10.1002/slct.202202062

Chemistry
Europe
European Chemical
Societies Publishing

enhancing the r_1 value. Besides, PMAO shell also plays an important role in the enhancement of contrast effect of Gd_2O_3 core because the presence of polar COO^- groups in each monomer of PMAO allows water molecules to easily pass through the coating layer and interact with Gd_2O_3. According to these results, it is clear that the $Gd_2O_3@PMAO$ nanoplates are potential candidates for *in vivo* MRI application.

Conclusion

The ultrathin Gd_2O_3 nanoplates with edge length and thickness around 10 nm and 1.1 nm, respectively, were successfully synthesized by the thermal decomposition method. The surface of the Gd_2O_3 nanoplates was modified by encapsulating with PMAO polymer as a biocompatible surface ligand. The superior coating stability was assessed under various experimental conditions by changing pH and saline concentration. The $Gd_2O_3@PMAO$ nanoplates exhibited good dispersion and stability in aqueous media for the long time (over 6 months) with hydrodynamic size of 32 nm. The longitudinal relaxivity rate r_1 of the Gd_2O_3 nanoplates is up to four times higher than that of the commercially available Gd-DTPA at 1.5T magnetic field. The in vitro cell viability test demonstrated that $Gd_2O_3@PMAO$ nanoplates are relatively safe in the range Gd_2O_3 concentration up to 100μg/ml. Although these results require further in vivo tests, they indicated that the PMAO coated-Gd_2O_3 nanoplates could be a potential candidate to use as an effective T_1 MRI contrast agent.

Supporting information summary

The Supporting Information includes the detailed experimental section of this work.

Acknowledgements

Conflict of Interest

The authors declare no conflict of interest.

Data Availability Statement

The data that support the findings of this study are available from the corresponding author upon reasonable request.

[1] S. Mornet, S. Vasseur, F. Grasset, E. Duguet, *J. Mater. Chem.* **2004**, *14*, 2161–2175.

[2] P. C. Wu, C. H. Su, F. Y. Cheng, J. C. Weng, J. H. Chen, T. L. Tsai, C. S. Yeh, W. C. Su, J. R. Hwu, Y. Tzeng, D. B. Shieh, *Bioconjugate Chem.* **2008**, *19*, 1972–1979.

[3] M. A. Hahn, A. K. Singh, P. Sharma, S. C. Brown, B. M. Moudgil, *Anal. Bioanal. Chem.* **2011**, *399*, 3–27.

[4] Z. Shen, W. Fan, Z. Yang, Y. Liu, V. I. Bregadze, S. K. Mandal, B. C. Yung, Li. Lin, T. Liu, W. Tang, L. Shan, Y. Liu, S. Zhu, S. Wang, W. Yang, L. H. Bryant, D. T. Nguyen, A. Wu, X. Chen, *Small* **2019**, *15*, 1903422.

[5] J. L. Major, T. J. Meade, *Acc. Chem. Res.* **2009**, *42*, 893–903.

[6] X. Y. Zheng, L. D. Sun, T. Zheng, H. Dong, Y. Li, Y. F. Wang, C. H. Yan, *Sci. Bull.* **2015**, *60*, 1092–1100.

[7] Y. Cao, L. J. Xu, Y. Kuang, D. S. Xiong, R. J. Pei, *J. Mater. Chem. B* **2017**, *5*, 3431.

[8] D. L. Ni, W. B. Bu, E. B. Ehlerding, W. B. Cai, J. L. Shi, *Chem. Soc. Rev.* **2017**, *46*, 7438.

[9] Y. Li, D. Xu, H. N. Chan, C. Y. Poon, S. L. Ho, H. W. Li, M. S. Wong, *Small* **2018**, *14*, 1800901.

[10] H. Hu, *Front. Chem.* **2020**, *8*, 1–20.

[11] H. B. Na, I. C. Song, T. Hyeon, *Adv. Mater.* **2009**, *21*, 2133–2148.

[12] S. Aime, M. Fasano, E. Terreno, *Chem. Soc. Rev.* **1998**, *27*, 19–29.

[13] P. Caravan, J. J. Ellison, T. J. McMurry, R. B. Lauffer, *Chem. Rev.* **1999**, *99*, 2293–2352.

[14] M. A. Fortin, R. M. Petoral Jr, F. Söderlind, A. Klasson, M. Engström, T. Veres, P. O. Käll, K. Uvdal, *Nanotechnology* **2007**, *18*, 395501.

[15] A. M. Morawski, G. A. Lanza, S. A. Wickline, *Curr. Opin. Biotechnol.* **2005**, *16*, 89–92.

[16] J. Q. Yuan, E. Peng, J. M. Xue, *J. Mater. Res.* **2014**, *29*, 1626–1634.

[17] C. H. Reynolds, N. Annan, K. Beshah, J. H. Huber, S. H. Shaber, R. E. Lenkinski, J. A. Wortman, *J. Am. Chem. Soc.* **2000**, *122*, 8940.

[18] P. J. Klemm, W. C. Floyd III, D. E. Smiles, J. M. J. Fréchet, K. N. Raymond, *Contrast Media Mol. Imaging* **2012**, *7*, 95–99.

[19] M. J. Cho, R. Sethi, J. S. A. Narayanan, S. S. Lee, D. N. Benoit, N. Taheri, P. Decuzzi, V. L. Colvin, *Nanoscale* **2014**, *6*, 13637.

[20] J. Wahsner, E. M. Gale, A. Rodriguez-Rodriguez, P. Caravan, *Chem. Rev.* **2019**, *119*, 957.

[21] W. Xu, K. Kattel, J. Y. Park, Y. Chang, T. J. Kim, G. H. Lee, *Phys. Chem. Chem. Phys.* **2012**, *14*, 12687–12700.

[22] N. Xiao, W. Gu, H. Wang, Y. L. Deng, X. Shi, L. Ye, *J. Colloid Interface Sci.* **2014**, *417*, 159.

[23] S. L. Mekuria, T. A. Debele, H. C. Tsai, *ACS Appl. Mater. Interfaces* **2017**, *9*, 6782–6795.

[24] F. Q. Hu, Y. S. Zhao, *Nanoscale* **2012**, *4*, 6235–6243.

[25] J. Fang, P. Chandrasekharan, X. L. Liu, Y. Yang, Y. B. Lv, C. T. Yang, J. Ding, *Biomaterials* **2014**, *35*, 1636–1642.

[26] H. Hifumi, S. Yamaoka, A. Tanimoto, D. Citterio, K. Suzuki, *J. Am. Chem. Soc.* **2006**, *128*, 15090–15091.

[27] J. Y. Park, M. J. Baek, E. S. Choi, S. Woo, J. H. Kim, T. J. Kim, J. C. Jung, K. S. Chae, Y. Chang, G. H. Lee, *ACS Nano* **2009**, *3*, 3663.

[28] A. A. Rahman, K. Vasilev, P. Majewski, *J. Colloid Interface Sci.* **2011**, *354*, 592–596.

[29] M. Ahren, L. Selegard, A. Klasson, F. Soderlind, N. Abrikossova, C. Skoglund, T. Bengtsson, M. Engstrom, P. Kall, K. Uvdal, *Langmuir* **2010**, *26*, 5753–5762.

[30] Z. Liu, X. Liu, Q. H. Yuan, K. Dong, L. Y. Jiang, Z. Q. Li, J. S. Ren, X. G. Qu, *J. Mater. Chem.* **2012**, *22*, 14982–14990.

[31] L. J. Zhou, Z. J. Gu, X. X. Liu, W. Y. Yin, G. Tian, L. Yan, S. Jin, W. L. Ren, G. M. Xing, W. Li, X. L. Chang, Z. B. Hu, Y. L. Zhao, *J. Mater. Chem.* **2012**, *22*, 966–974.

[32] M. W. Ahmad, W. Xu, S. J. Kim, J. S. Baeck, Y. Chang, J. E. Bae, K. S. Chae, J. A. Park, T. J. Kim, G. H. Lee, *Sci. Rep.* **2015**, *5*, 8549.

[33] K. Y. Ni, Z. H. Zhao, Z. J. Zhang, Z. J. Zhou, L. Yang, L. R. Wang, H. Ai, J. H. Gao, *Nanoscale* **2016**, *8*, 3768–3774.

[34] X. Miao, S. L. Ho, T. Tegafaw, H. Cha, Y. Chang, I. T. Oh, A. M. Yaseen, S. Marasini, A. Ghazanfari, H. Yue, K. S. Chae, G. H. Lee, *RSC Adv.* **2018**, *8*, 3189.

[35] M. Y. Ahmad, M. W. Ahmad, H. Yue, S. L. Ho, J. A. Park, K. H. Jung, H. Cha, S. Marasini, A. Ghazanfari, S. Liu, T. Tegafaw, K. S. Chae, Y. Chang, G. H. Lee, *Molecules* **2020**, *25*, 1159.

[36] Z. Zhou, R. Hu, L. Wang, C. Sun, G. Fu, J. Gao, *Nanoscale* **2016**, *8*, 17887–17894.

[37] D. Wang, D. Kang, X. Ye, C. B. Murray, *Chem. Mater.* **2014**, *26*, 6328.

[38] E. Jung, T. Yu, W. S. Kim, *Korean J. Chem. Eng.* **2016**, *33*, 683–687.

[39] W. Cai, Y. Zhang, J. Wang, Z. Wang, Y. Tian, H. Liu, H. Pan, L. Fu, W. Chen, C. Wu, X. Wang, G. Liu, *Chem. Eng. J.* **2020**, *380*, 122473.

[40] G. Stinnett, N. Taheri, J. Villanova, A. Bohloul, X. Guo, E. P. Esposito, Z. Xiao, D. Stueber, C. Avendano, P. Decuzzi, R. G. Pautler, V. L. Colvin, *Adv. Healthcare Mater.* **2021**, *10*, 2001780.

[41] Z. Zhou, Z. H. Zhao, H. Zhang, Z. Wang, X. Chen, R. Wang, Z. Chen, J. Gao, *ACS Nano* **2014**, *8*, 7976- 7985.

[42] Z. Zhou, C. Wu, H. Liu, X. Zhu, Z. Zhao, L. Wang, Y. Xu, H. Ai, J. Gao, *ACS Nano* **2015**, *9*, 3012-3022.

[43] Y. C. Cao, *J. Am. Chem. Soc.* **2004**, *126*, 7456.

[44] Z. Zhao, K. Xu, C. Fu, H. Liu, M. Lei, J. Bao, A. Fu, Y. Yu, W. Zhang, *Biomaterials* **2019**, *219*, 119379.

[45] R. Di Corato, A. Quarta, P. Piacenza, A. Ragusa, A. Figuerola, R. Buonsanti, R. Cingolani, L. Manna, T. Pellegrino, *J. Mater. Chem.* **2008**, *18*, 1991.

[46] G. C. Lavorato, J. C. Azcárate, M. B. R. Aiello, J. M. O. Henao, P. M. Zélis, M. Ceolin, E. Winkler, M. H. Fonticelli, C. Vericat, *Appl. Surf. Sci.* **2021**, *570*, 151171.

[47] E. Peng, E. S. G. Choo, C. S. H. Tan, X. Tang, Y. Sheng, J. Xue, *Nanoscale* **2013**, *5*, 5994–6005.

[48] H. Molaei, F. Zaaeri, S. Sharifi, S. Ramazani, S. Safaei, J. Abdolmohammadi, M. Khoobi, *Int. J. Polym. Mater. Polym. Biomater.* **2021**, *70*, 1344–1353.

[49] N. T. Dung, N. V. Long, L. T. T. Tam, P. H. Nam, L. D. Tung, N. X. Phuc, L. T. Lu, N. T. K. Thanh, *Nanoscale* **2017**, *9*, 8952–8961.

[50] P. H. Nam, L. T. Lu, P. H. Linh, D. H. Manh, L. T. T. Tam, N. X. Phuc, P. T. Phong, I. J. Lee, *New J. Chem.* **2018**, *42*, 14530.

[51] M. Rohrer, H. Bauer, J. Mintorovitch, M. Requardt, H. J. Weinmann, *Invest. Radiol.* **2005**, *40*, 715–724.

[52] A. Hedlund, M. Ahrén, H. Gustafsson, N. Abrikossova, M. Warntjes, J. I. Jönsson, K. Uvdal, M. Engström, *Int. J. Nanomed.* **2011**, *6*, 3233.

[53] L. Faucher, M. Tremblay, J. Lagueux, Y. Gossuin, M. A. Fortin, *ACS Appl. Mater. Interfaces* **2012**, *4*, 4506.

[54] N. Q. Luo, X. M. Tian, C. Yang, J. Xiao, W. Y. Hu, D. H. Chen, L. Li, *Phys. Chem. Chem. Phys.* **2013**, *15*, 12235–12240.

[55] J. Yuan, E. Peng, J. M. Xue, *J. Mater. Res.* **2014**, *29*, 1626–1634.

[56] X. Miao, W. Xu, H. Cha, Y. Chang, I. T. Oh, K. S. Chae, T. Tegafawa, S. L. Hoa, S. J. Kim, G. H. Lee, *Appl. Surf. Sci.* **2017**, *477*, 111–115.